Prediction of Intrinsic Ferromagnetic Ferroelectricity in a Transition-Metal Halide Monolayer

Chengxi Huang,[1,2] Yongping Du,[1] Haiping Wu,[1,*] Hongjun Xiang,[3,4,†] Kaiming Deng,[1] and Erjun Kan[1,2,‡]
[1]Department of Applied Physics and Institution of Energy and Microstructure, Nanjing University of Science and Technology, Nanjing, Jiangsu 210094, People's Republic of China
[2]Key Laboratory of Soft Chemistry and Functional Materials (Ministry of Education), Nanjing University of Science and Technology, Nanjing, Jiangsu 210094, People's Republic of China
[3]Key Laboratory of Computational Physical Sciences (Ministry of Education), State Key Laboratory of Surface Physics, and Department of Physics, Fudan University, Shanghai 200433, People's Republic of China
[4]Collaborative Innovation Center of Advanced Microstructures, Nanjing 210093, People's Republic of China

(Received 7 June 2017; revised manuscript received 25 September 2017; published 2 April 2018)

The realization of multiferroics in nanostructures, combined with a large electric dipole and ferromagnetic ordering, could lead to new applications, such as high-density multistate data storage. Although multiferroics have been broadly studied for decades, ferromagnetic ferroelectricity is rarely explored, especially in two-dimensional (2D) systems. Here we report the discovery of 2D ferromagnetic ferroelectricity in layered transition-metal halide systems. On the basis of first-principles calculations, we reveal that a charged $CrBr_3$ monolayer exhibits in-plane multiferroicity, which is ensured by the combination of orbital and charge ordering as realized by the asymmetric Jahn-Teller distortions of octahedral Cr—Br_6 units. As an example, we further show that $(CrBr_3)_2Li$ is a ferromagnetic ferroelectric multiferroic. The explored phenomena and mechanism of multiferroics in this 2D system not only are useful for fundamental research in multiferroics but also enable a wide range of applications in nanodevices.

DOI: 10.1103/PhysRevLett.120.147601

Multiferroics, which simultaneously exhibit ferroelectricity and magnetism, have received intensive studies because of their novel physics and potential applications for spintronics and memory devices [1–4]. Until now, two kinds of multiferroics have been well discovered. In the type-I multiferroics, the ferroelectricity and magnetic ordering have different sources, which usually results in a weak magnetoelectric (ME) coupling. In the type-II multiferroics, the ferroelectricity is caused by the magnetic ordering which breaks the centrosymmetry. In this case, the ME coupling is strong, but the electric polarization is usually very small and the transition temperature is quite low [3,4]. Two-dimensional (2D) materials with robust ferroelectric (FE) as well as ferromagnetic (FM) order are promising materials for multifunctional applications but are rather scarce [5,6] because of the inherent exclusion between ferroelectricity and ferromagnetism [3,7]. Actually, up to now, 2D FM FE systems have not been reported yet.

Recently, ferroelectricity in 2D materials was discovered. For example, 1*T* MoS_2 [8], functionalized graphene [9], SnSe [10], phosphorene [11,12], phosphorus oxides [13], and In_2Se_3 [14] are theoretically predicted to be 2D FE materials. Moreover, Chang *et al.* have experimentally shown that a tin telluride (SnTe) monolayer has robust FE properties [15]. Also, 2D ferromagnetism has been experimentally observed in two transition-metal compound layered systems, i.e., $Cr_2Ge_2Te_6$ [16] and CrI_3 [17]. The family of transition-metal halides (TMHs) has received much attention because of their interesting topological and spintronic properties [17–25]. Note that most of the TMHs are magnetic semiconductors or insulators. These exciting discoveries have motivated us to explore the possibility of the coexistence of ferromagnetism and ferroelectricity in a single 2D system, e.g., a TMH monolayer.

Here, in this work, by studying an example system of the TMH monolayers ($CrBr_3$), we discover that multiferroicity could be induced by the combination of charge order (CO) and orbital order (OO). Based on first-principles calculations, our results show that, by doping one electron in the $CrBr_3$ primitive cell, the anomalous asymmetric Jahn-Teller (JT) distortions of two neighboring Cr—Br_6 units bring simultaneously CO and OO. The resulting spatial electron-hole separation and spontaneous symmetry breaking will lead to 2D multiferroicity in the $CrBr_3^{0.5-}$ system. We further investigate the FM and FE properties of $(CrBr_3)_2Li$, in which the Li^+ cations are adopted as electron donors. Finally, we discuss the possible multiferroicity in other TMH systems.

Our first-principles calculations are based on the density functional theory (DFT) as implemented in the Vienna *ab initio* simulations package (VASP) [26]. The exchange-correlation functional proposed by Perdew, Burke, and Ernzerhof [27] was used. The effective Hubbard $U = 3$ eV was added according to Dudarev's method [28] for the Cr-*d*

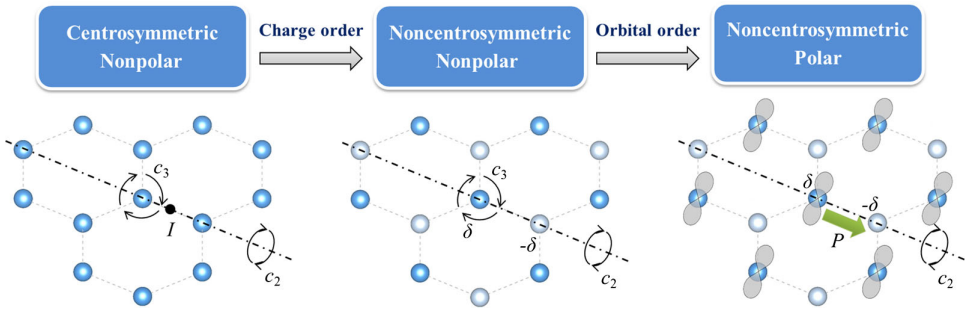

FIG. 1. Evolution from a nonpolar to a polar honeycomb structure driven by the combination of CO and OO.

orbitals. The projector augmented wave method [29] was used to treat the core electrons. The plane-wave cutoff energy was set to be 500 eV, and the first Brillouin zone was sampled using a Γ-centered $12 \times 12 \times 1$ Monkhorst-Pack grid [30]. A vacuum space of 20 Å was adopted, and the FE polarization was calculated using the Berry phase method [31].

Ferroelectricity originates from the separation between negative and positive charges. Previous studies have shown that either CO or OO [32–36] can lead to ferroelectricity in 3D systems. However, in some systems, individual CO or OO cannot ensure the appearance of ferroelectricity. For instance, in a 2D honeycomb lattice with a uniform charge distribution (Fig. 1), the existence of centrosymmetry makes it nonpolar. If δ charges transfer from one sublattice to the other one, a CO phase is formed, but the system is still nonpolar because of the in-plane $c_{3\perp}$ symmetry. Then if we further induce OO in this system, which breaks the in-plane $c_{3\perp}$ symmetry, an in-plane electric polarization will occur. Thus, in this case, the combination of CO and OO is responsible for the appearance of ferroelectricity.

One of the candidate systems to study the CO-OO-cooperating ferroelectricity is $CrBr_3$. The $CrBr_3$ monolayer shown in Fig. 2(a) (point group D_{3d}) is a nonpolar FM insulator. In the cases of hole doping, the $CrBr_3^{x+}$ ($0 < x \leq 0.5$) systems keep the D_{3d} symmetry, while for electron doping, a remarkable JT distortion in $CrBr_3^{x-}$ appears, resulting in a structure with a polar C_2 symmetry. This dramatic difference can be understood. In the case of hole doping, the Fermi level of $CrBr_3$ shifts downward into the bands dominated by Br-p orbitals. Thus, no JT distortions appear. In the case of electron doping, the Fermi level shifts upward, leading to partially occupied Cr-e states, where JT distortions occur to break the degeneracy and stabilize the system [Fig. 2(f)].

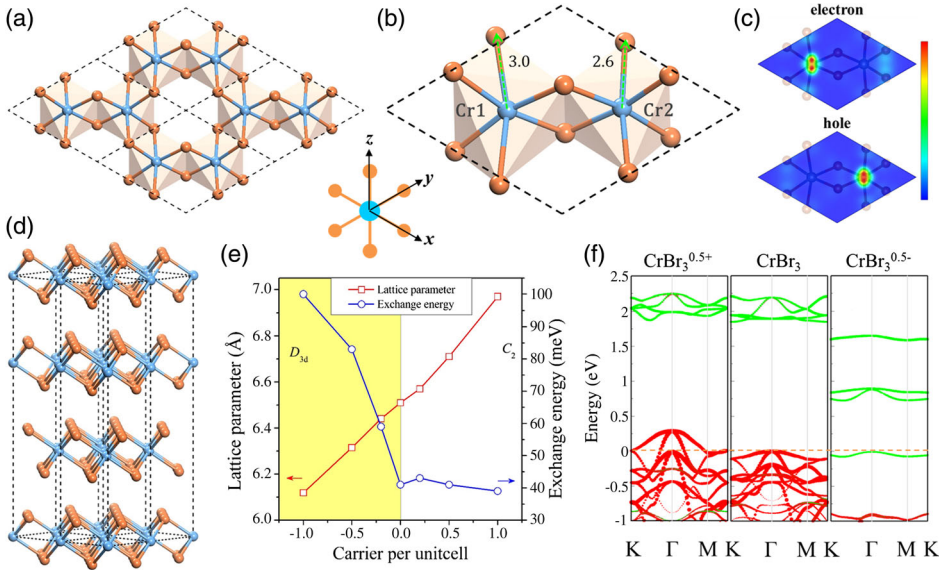

FIG. 2. Top view of the optimized $CrBr_3$ (a) and $CrBr_3^{0.5-}$ (b) monolayer. Brown and cyan balls represent Br and Cr atoms, respectively. The dashed rhombus represents the primitive cell. (c) Electron and hole density in real space for the valence band maximum and the conduction band minimum, respectively. Red and blue represent the maximum and minimum value, respectively. (d) Pristine $CrBr_3$ bulk. (e) Lattice parameter and exchange energy ($E_{AFM} - E_{FM}$) per unit cell refer to carrier concentration. Negative and positive values of the carrier concentration represent hole and electron doping, respectively. (f) Orbital-resolved band structures for $CrBr_3^{0.5+}$, $CrBr_3$, and $CrBr_3^{0.5-}$. Green lines represent Cr-d states. Red lines represent Br-p states.

The optimal structure of $CrBr_3^{0.5-}$ is shown in Fig. 2(b). Interestingly, the distortions of two neighboring Cr—Br_6 units are not equal. In the Cr1 − Br_6 unit, the two Cr—Br bonds along the z direction (∼3.0 Å) are much longer than the other four (∼2.6 Å). In the Cr2—Br_6 unit, the distortions are less obvious. This is quite anomalous compared to the common JT distortions in pristine TMHs [37]. We name these two kinds of distortions "asymmetric distortions" and "symmetric distortions," respectively. We also calculated the $CrBr_3^{0.5-}$ systems with fixed D_{3d} (with no JT distortions) and C_{2h} (with symmetric JT distortions) symmetries. The results show that both D_{3d}-(0.26 eV) and C_{2h}-$CrBr_3^{0.5-}$ (0.11 eV) are much higher in energy than the C_2-$CrBr_3^{0.5-}$ (Fig. S1 [38]). Moreover, our DFT + U (U = 1–4 eV) and HSE06 calculations give similar results, and the dynamical stability of C_2-$CrBr_3^{0.5-}$ is verified by phonon calculations (Fig. S2 [38]).

The formal oxidation state of Cr1 and Cr2 is +2 and +3, with magnetic moments of 4 and 3μ_B, respectively. A CO phase is clearly observed [Fig. 2(c)]. The FM order is more favored than the antiferromagnetic (AFM) order (two neighboring spins are antiparallel). Zhou and Sun have demonstrated that electron doping could enhance the FM coupling in a 2D organometallic system [47]. In $CrBr_3$, electron doping causes asymmetric JT distortions, greatly changing the electronic structures (e.g., split of Cr-e states) near the Fermi level as well as the magnetic coupling.

Because of the asymmetric JT distortions, the electric polarization of C_2-$CrBr_3^{0.5-}$ occurs parallel to the in-plane c_2 axis, which is perpendicular to the occupied Cr1-dz^2 orbital. To reveal the origin of the in-plane polarization, we considered two similar hypothetical systems, i.e., $CrFeBr_6$ (replace one Cr to Fe atom in the $CrBr_3$ unit cell) and $MnBr_3$ (replace all Cr to Mn atoms). The optimized structure of $CrFeBr_6$ belongs to D_3 symmetry, where no JT distortion is observed. The magnetic moments of Fe^{3+} and Cr^{3+} are 5 and 3μ_B, respectively. Thus, the D_3-$CrFeBr_6$ can be considered to have CO but no OO. For $MnBr_3$, the optimized structure belongs to C_{2h} symmetry, and JT distortions equally appear in each Mn—Br_6 unit. The magnetic moment of each Mn^{3+} is 4μ_B. Thus, the C_{2h}-$MnBr_3$ has OO but no CO. In C_2-$CrBr_3^{0.5-}$, because of the asymmetric JT distortions, CO and OO phases are simultaneously formed. However, we find that both D_3-$CrFeBr_6$ and C_{2h}-$MnBr_3$ are nonpolar; only C_2-$CrBr_3^{0.5-}$ is polar. Therefore, the in-plane polarization of C_2-$CrBr_3^{0.5-}$ is driven by the combination of CO and OO. To verify the spontaneous symmetry breaking in $CrBr_3^{0.5-}$, we also plotted the phonon dispersions of the nonpolar phases, namely, D_{3d}-, C_{2h}-, and D_3-$CrBr_3^{0.5-}$ (Fig. S2 [38]), in which the imaginary bands of soft optical modes are observed [48]. The relation between JT distortions and ferroelectricity has also been studied in perovskite systems [49], which may allow electric field control of the structural and electronic properties.

To explain why the asymmetric JT distortions are preferred over the symmetric JT distortions in $CrBr_3^{0.5-}$, we start from the degenerated Cr-e states derived from the octahedral ligand field. In C_{2h}-$CrBr_3^{0.5-}$, Cr-e states of two Cr—Br_6 units equally split to higher $dx^2 - y^2$ and lower dz^2 states. The added electron occupies the bonding state generated from the hybridization between Cr1- and Cr2-dz^2 states [Figs. 3(a) and 3(c)]. The average valence for Cr is +2.5. In this case, the electronic energy benefits from two parts, i.e., the split of Cr-e states and hybridizations between Cr-dz^2 orbitals. In C_2-$CrBr_3^{0.5-}$, distortions in the Cr1—Br_6 unit are much stronger than that in Cr2—Br_6, leading to an unequal split of two Cr-e states. The lower Cr1-dz^2 state hardly hybridizes with the higher Cr2-dz^2 state. Then the Cr1-dz^2 state is occupied by the added electron, while the Cr2-dz^2 state is empty [Figs. 3(b) and 3(d)]. The electronic energy benefits only from the split of the Cr1-e state. As we know, the 3d orbitals are much localized. Thus, the direct hybridizations between Cr-dz^2 orbitals can be omitted. The electronic energy benefits are mainly decided by the strength of the split of Cr-e states. From Figs. 3(c) and 3(d), one finds that the split of Cr1-e states from asymmetric distortions (∼1.6 eV in energy) is much larger than that from symmetric distortions (∼0.8 eV in energy), which explains why asymmetric distortions are preferred in this system.

Magnetic anisotropy (MA) and ME coupling in C_2-$CrBr_3^{0.5-}$ is examined by including the spin-orbit coupling (SOC). The pristine $CrBr_3$ monolayer has an out-of-plane magnetic easy axis [24]. However, in C_2-$CrBr_3^{0.5-}$, the easy axis is within the atomic plane, parallel to the in-plane

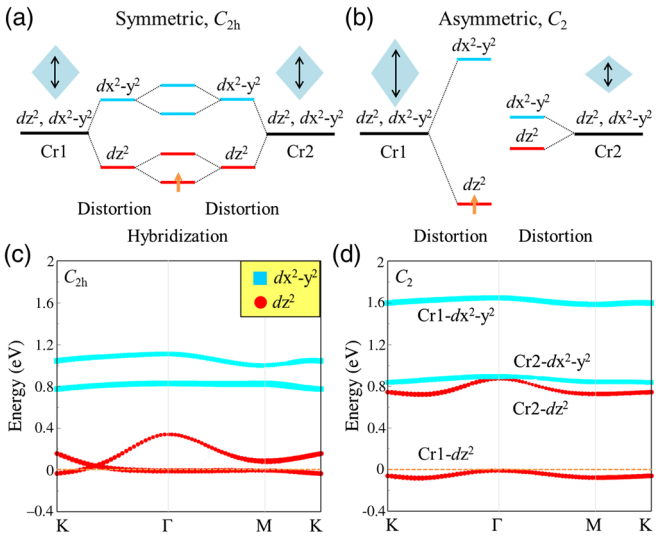

FIG. 3. Evolution of states under symmetric (a) and asymmetric (b) JT distortions. Blue rhombuses represent the distorted octahedral ligand field for each Cr—Br_6 sublattice. Orbital-resolved bands around the Fermi level for $CrBr_3^{0.5-}$ with C_{2h} (c) and C_2 (d) symmetry.

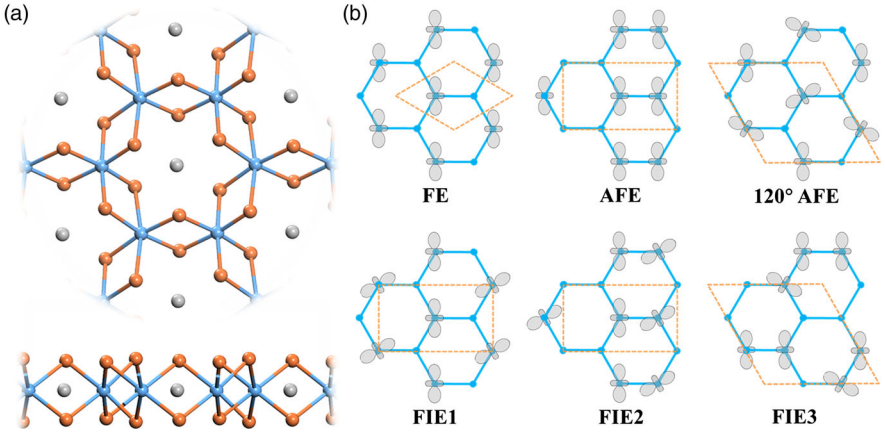

FIG. 4. (a) Top and side view of the optimized $(CrBr_3)_2Li$ monolayer. Brown, cyan, and gray balls represent Br, Cr, and Li atoms, respectively. (b) Schematic diagrams of FE, AFE, and FIE orders. Blue framworks represent the honeycomb sublattice. Gray graphs represent the occupied Cr-dz^2 orbital. Orange dashed frames represent unit cells of structures with corresponding polarization orders.

polarization. This implies that the in-plane FE order is coupled with the net magnetization. Moreover, according to the combinations of different CO and OO, there should be six possible orientations of the in-plane FE order, i.e., 0°, 60°, 120°, 180°, 240°, and 300° orientations (Fig. S3 [38]).

After studying the hypothetical $CrBr_3^{0.5-}$ system, we now turn to the realistic materials feasible in experiments. There are many ways to dope electrons into a 2D system, such as using a substrate, doping metals, or ions. Lei *et al.* have achieved a high-density (Li/Fe ratio up to 0.5) carrier doping in a layered FeSe thin film by using Li^+ [50]. Here we also choose Li^+ as electron donors. Four possible adsorption sites of Li^+ on the $CrBr_3$ monolayer are considered (Fig. S4 [38]), and the hole center of the porous $CrBr_3$ framework is preferred by the dopant [Fig. 4(a)]. In $(CrBr_3)_2Li$ (C_2 point group), large asymmetric distortions take place in the $CrBr_3$ framework. The lateral lattice parameter is 6.49 Å, and the angle between a and b lattice vectors is 118.6°. Its thermal stability is examined by performing *ab initio* molecular dynamics simulations at 300 K (Fig. S6 [38]).

To further confirm the ferroelectricity in $(CrBr_3)_2Li$, we considered four possible configurations [namely, FE, antiferroelectric (AFE), and ferrielectric (FIE1 and FIE2) orders; see Fig. 4(b)] in a 2×1 supercell containing four $Cr{-}Br_6$ units. The AFE structure is found to have higher energy (~21.3 meV per Cr) than the FE structure, while the FIE1 and FIE2 structures always automatically converge into the FE and AFE structures, respectively. Furthermore, we considered two typical orders in a $\sqrt{3} \times \sqrt{3}$ supercell containing six $Cr{-}Br_6$ units, namely, the 120° AFE and FIE3 order [Fig. 4(b)]. The relative energies of 120° AFE and FIE3 structure are ~9.0 and ~22.3 meV, respectively, per Cr with respect to the FE structure. We have also considered two other similar $CrBr_3^{0.5-}$ systems, namely, $(CrBr_3)_2NH_4$ and $(CrBr_3)_2Na$ (Fig. S4–S7 [38]), and find that the 120° AFE structures have the lowest energy (Table S2 [38]). These imply that whether the FE order is favored in $CrBr_3^{0.5-}$ systems or not depends on the properties (e.g., size) of the electron donors.

The same as $CrBr_3^{0.5-}$, the magnetic ground state of the FE $(CrBr_3)_2Li$ monolayer is FM with an exchange energy ($\Delta E = E_{\mathrm{AFM}} - E_{\mathrm{FM}}$) of ~15 meV per Cr. The magnetic moments of two neighboring Cr are 4 and $3\mu_B$, respectively. Including SOC, the easy axis is parallel to the in-plane polarization. The MA energies are 87 (with respect to in-plane hard axis) and 82 μeV (with respect to out-of-plane hard axis) per Cr, respectively. These values are larger than those of traditional metals such as Fe (1.4 μeV). Because of the non-negligible uniaxial MA, here we use the Heisenberg model including single ion anisotropy to describe the magnetic behavior of this system. The spin Hamiltonian

$$H = -J\sum_{\langle ij\rangle} S_i S_j - D\sum_{\langle i\rangle} S_{i,x0}^2,$$

where J represents the nearest-neighbor exchange coupling, D represents the single-ion anisotropy parameter, and $S_{i,x0}$ represents the component of S_i along the in-plane easy-axis ($x0$) direction. The values of J and D are calculated to be ~1661 and ~14 μeV, respectively. The T_C is estimated to be ~50 K by classic Monte Carlo simulations [51]. The behaviors of M_{x0} and M_{tot} are very close, indicating that the MA in this system is large enough to stabilize the orientation of net magnetization below the T_C.

The in-plane spontaneous polarization of FE order is calculated to be 0.92×10^{-10} C/m for $(CrBr_3)_2Li$. If we take the thickness to be 6 Å, which is close to the interlayer space of bulk $CrBr_3$, the value will be ~15 $\mu C/cm^2$. This value is comparable to those of recently reported 2D FE SnSe, phosphorene [10–12], and $BaTiO_3$ bulk [44,52]. As mentioned above, there are six possible orientations of in-plane FE order in the $(CrBr_3)_2Li$. Here we explore the

representative 120° FE switching by the nudged-elastic-band (NEB) method (Fig. S9 [38]). The switching barrier is estimated to be ~15 meV/unit cell, comparable to that of tetragonal bulk $BaTiO_3$ (~18 meV/unit cell from our calculations). The ME coupling in $(CrBr_3)_2Li$ is also studied by the 120° FE switching, during which the orientation of magnetization is controlled by the electric field. The ME coupling coefficient is estimated to be in the same order as those in $Fe/BaTiO_3$ [45] and $BiFeO_3/CoFe_2O_4$ interfaces [46] (see Fig. S10 [38] for details).

For practical interests, it is necessary to examine whether the inherent properties of a 2D material could be affected by the substrate. Here we choose two nonmagnetic nonpolar insulators, namely, the β-tridymite SiO_2 and α-$InBr_3$ slabs to support the $(CrBr_3)_2Li$ monolayer. After structural optimizations, the significant asymmetric JT distortions and in-plane ferroelectricity are observed in the $(CrBr_3)_2Li$ layer. The ground states are FM, and the Cr-dz^2 and Cr-dx^2-y^2 bands are located within the large energy gap of the substrates. Thus, we expect that the FM-FE multiferroic features of the $(CrBr_3)_2Li$ monolayer can persist on a suitable substrate (see [38] for details).

At last, we discuss the possibility of multiferroicity in other charged TMH systems. First of all, CrX_3 (X = Cl, I) has very similar atomic (honeycomb framework consists of octahedral Cr-X_6 sublattices) and electronic structures (occupied t_{2g} and empty e_g in one spin channel) as $CrBr_3$. Our calculations show that the asymmetric JT distortions and multiferroic features also occur in $CrCl_3^{0.5-}$ and $CrI_3^{0.5-}$ (Fig. S12 [38]). Second, in some TMHs which exhibit inherent JT distortions with a mirror symmetry in their bulk phases such as $RhCl_3$ and $RhBr_3$, doping either electrons or holes could break the mirror symmetry and induce in-plane electric polarizations as well as magnetism. It appears that electronic correlations may play an important role in the occurrence of asymmetric instead of symmetric JT distortions. Overall, we suggest that 2D multiferroicity could widely exist in the family of TMHs, which may offer a new promising platform to study 2D multiferroics.

In summary, based on first-principles calculations, we reveal that the $CrBr_3^{0.5-}$ monolayer systems are 2D multiferroic semiconductors with in-plane FM and FE orders. The orientation of in-plane net magnetization is coupled with the electric polarization, evidencing the existence of ME coupling. An example material system [i.e., the $(CrBr_3)_2Li$ monolayer] is predicted to be a FM-FE multiferroic. In these systems, the in-plane ferroelectricity is ensured by the combination of CO and OO, which are induced by the asymmetric JT distortions of two neighboring Cr-Br_6 units. This mechanism is not restricted to the $CrBr_3^{0.5-}$ systems but can also be applied to other TMHs and related 2D systems. These findings reveal the existence of multiferroicity in 2D systems and provide a new ideal platform to study 2D multiferroics. We are looking forward to future experimental realizations of 2D multiferroics in TMH systems.

E. K. is supported by the NSFC (51522206, 51790492,11574151, 11774173), by NSF of Jiangsu Province (BK20130031), by PAPD, the Fundamental Research Funds for the Central Universities (No. 30915011203), and by New Century Excellent Talents in University (NCET-12-0628). Work at Fudan is supported by NSFC, the Special Funds for Major State Basic Research (2015CB921700), Program for Professor of Special Appointment (Eastern Scholar), Qing Nian Ba Jian Program. C. H. and E. K. acknowledge the support from the Tianjing Supercomputer Centre and Shanghai Supercomputer Center. We thank Jian Zhou for valuable discussions.

*To whom all correspondence should be addressed.
mrhpwu@njust.edu.cn
†hxiang@fudan.edu.cn
‡ekan@njust.edu.cn

[1] W. Eerenstein, N. D. Mathur, and J. F. Scott, Nature (London) **442**, 759 (2006).
[2] S.-W. Cheong and M. Mostovoy, Nat. Mater. **6**, 13 (2007).
[3] K. F. Wang, J.-M. Liu, and Z. F. Ren, Adv. Phys. **58**, 321 (2009).
[4] S. Dong, J.-M. Liu, S.-W. Cheong, and Z. Ren, Adv. Phys. **64**, 519 (2015).
[5] R. Ramesh and N. A. Spaldin, Nat. Mater. **6**, 21 (2007).
[6] J. H. Lee *et al.* Nature (London) **466**, 954 (2010).
[7] N. A. Spaldin, S.-W. Cheong, and R. Ramesh, Phys. Today **63**, No. 10, 38 (2010).
[8] S. N. Shirodkar and U. V. Waghmare, Phys. Rev. Lett. **112**, 157601 (2014).
[9] E. Kan, F. Wu, K. Deng, and W. Tang, Appl. Phys. Lett. **103**, 193103 (2013).
[10] R. Fei, W. Kang, and L. Yang, Phys. Rev. Lett. **117**, 097601 (2016).
[11] M. Wu and X. C. Zeng, Nano Lett. **16**, 3236 (2016).
[12] T. Hu, H. Wu, H. Zeng, K. Deng, and E. Kan, Nano Lett. **16**, 8015 (2016).
[13] W. Luo and H. Xiang, Angew. Chem., Int. Ed. **128**, 8717 (2016).
[14] W. Ding, J. Zhu, Z. Wang, Y. Gao, D. Xiao, Y. Gu, Z. Zhang, and W. Zhu, Nat. Commun. **8**, 14956 (2017).
[15] K. Chang, J. Liu, H. Lin, N. Wang, K. Zhao, A. Zhang, F. Jin, Y. Zhong, X. Hu, W. Duan, Q. Zhang, L. Fu, Q.-K. Xue, X. Chen, and S.-H. Ji, Science **353**, 274 (2016).
[16] C. Gong *et al.*, Nature (London) **546**, 265 (2017).
[17] B. Huang *et al.*, Nature (London) **546**, 270 (2017).
[18] M. A. McGuire, H. Dixit, V. R. Cooper, and B. C. Sales, Chem. Mater. **27**, 612 (2015).
[19] J. He, S. Ma, P. Lyu, and P. Nachtigall, J. Mater. Chem. C **4**, 2518 (2016).
[20] A. Banerjee, C. A. Bridges, J.-Q. Yan, A. A. Aczel, L. Li, M. B. Stone, G. E. Granroth, M. D. Lumsden, Y. Yiu, J. Knolle, S. Bhattacharjee, D. L. Kovrizhin, R. Moessner,

D. A. Tennant, D. G. Mandrus, and S. E. Nagler, Nat. Mater. **15**, 733 (2016).
[21] P. Zhou, C. Q. Sun, and L. Z. Sun, Nano Lett. **16**, 6325 (2016).
[22] C. Huang, J. Zhou, H. Wu, K. Deng, P. Jena, and E. Kan, Phys. Rev. B **95**, 045113 (2017).
[23] V. Nicolosi, M. Chhowalla, M. G. Kanatzidis, M. S. Strano, and J. N. Coleman, Science **340**, 1226419 (2013).
[24] W.-B. Zhang, Q. Qu, P. Zhu, and C.-H. Lam, J. Mater. Chem. C **3**, 12457 (2015).
[25] J. Liu, Q. Sun, Y. Kawazoe, and P. Jena, Phys. Chem. Chem. Phys. **18**, 8777 (2016).
[26] G. Kresse and J. Hafner, Phys. Rev. B **47**, 558 (1993).
[27] J. P. Perdew, K. Burke, and M. Ernzerhof, Phys. Rev. Lett. **77**, 3865 (1996).
[28] S. L. Dudarev, G. A. Botton, S. Y. Savrasov, C. J. Humphreys, and A. P. Sutton, Phys. Rev. B **57**, 1505 (1998).
[29] P. E. Blöchl, Phys. Rev. B **50**, 17953 (1994).
[30] H. J. Monkhorst and J. D. Pack, Phys. Rev. B **13**, 5188 (1976).
[31] R. D. King-Smith and D. Vanderbilt, Phys. Rev. B **47**, 1651 (1993).
[32] K. Xu and H. J. Xiang, Phys. Rev. B **92**, 121112 (2015).
[33] K. Singh, C. Simon, E. Cannuccia, M.-B. Lepetit, B. Corraze, E. Janod, and L. Cario, Phys. Rev. Lett. **113**, 137602 (2014).
[34] N. Ikeda, H. Ohsumi, K. Ohwada, K. Ishii, T. Inami, K. Kakurai, Y. Murakami, K. Yoshii, S. Mori, Y. Horibe, and H. Kitô, Nature (London) **436**, 1136 (2005).
[35] K. Gupta, P. Mahadevan, P. Mavropoulos, and M. Ležaić, Phys. Rev. Lett. **111**, 077601 (2013).
[36] K. Yamauchi and P. Barone, J. Phys. Condens. Matter **26**, 103201 (2014).
[37] H. Bengel, H. J. Cantow, S. N. Magonov, H. Hillebrechtb, G. Thieleb, W. Liangc, and M. H. Whangbo, Surf. Sci. **343**, 95 (1995).
[38] See Supplemental Material at http://link.aps.org/supplemental/10.1103/PhysRevLett.120.147601, which includes Refs. [39–46], for structural details and relative energies of D_{3d}-, C_{2h}-, and D_3-$CrBr_3^{0.5-}$, phonon spectra, Hubbard U effects, and orientations of ferroelectric order for C_2-$CrBr_3^{0.5-}$, adsorption configurations and relative energies, structural details, AIMD simulation results, band structures, Monte Carlo simulation results, relative energies of different in-plane polarization orders and NEB results for $(CrBr_3)_2NH_4$, $(CrBr_3)_2Na$, and $(CrBr_3)_2Li$, detailed results on magnetoelectric coupling and the substrate effect for $(CrBr_3)_2Li$, and structural details for C_2-$CrCl_3^{0.5-}$ and $CrI_3^{0.5-}$.
[39] J. Íñiguez, Phys. Rev. Lett. **101**, 117201 (2008).
[40] E. Bousquet, N. A. Spaldin, and K. T. Delaney, Phys. Rev. Lett. **106**, 107202 (2011).
[41] J. T. Heron, M. Trassin, K. Ashraf, M. Gajek, Q. He, S. Y. Yang, D. E. Nikonov, Y. H. Chu, S. Salahuddin, and R. Ramesh, Phys. Rev. Lett. **107**, 217202 (2011).
[42] C.-G. Duan, J. P. Velev, R. F. Sabirianov, Z. Zhu, J. Chu, S. S. Jaswal, and E. Y. Tsymbal, Phys. Rev. Lett. **101**, 137201 (2008).
[43] B. Xu, V. Garcia, S. Fusil, M. Bibes, and L. Bellaiche, Phys. Rev. B **95**, 104104 (2017).
[44] K. J. Choi, M. Biegalski, Y. L. Li, A. Sharan, J. Schubert, R. Uecker, P. Reiche, Y. B. Chen, X. Q. Pan, V. Gopalan, L.-Q. Chen, D. G. Schlom, and C. B. Eom, Science **306**, 1005 (2004).
[45] C.-G. Duan, S. S. Jaswal, and E. Y. Tsymbal, Phys. Rev. Lett. **97**, 047201 (2006).
[46] F. Zavaliche *et al.*, Nano Lett. **5**, 1793 (2005).
[47] J. Zhou and Q. Sun, Nanoscale **6**, 328 (2014).
[48] P. A. Fleury, J. F. Scott, and J. M. Worlock, Phys. Rev. Lett. **21**, 16 (1968).
[49] J. Varignon, N. C. Bristowe, and P. Ghosez, Phys. Rev. Lett. **116**, 057602 (2016).
[50] B. Lei *et al.* Phys. Rev. B **95**, 020503 (2017).
[51] P. S. Wang, W. Ren, L. Bellaiche, and H. J. Xiang, Phys. Rev. Lett. **114**, 147204 (2015).
[52] X. Wu, K. M. Rabe, and D. Vanderbilt, Phys. Rev. B **83**, 020104 (2011).